Scintillating Fibre Detectors using Position-Sensitive Photomultipliers

FAROS Collaboration

V. Agoritsas[+], N. Akchurin[#], A. M. Bergdolt[##], O. Bing[##], A. Bravar[#::], A. Cardini[**oo],

J. Ditta[*], S. Dolinski[**], R. Drevenak[o], J. Dufournaud[*], Mic. Finger[o"], Mir. Finger[*o],

V. Flaminio[**], B. Di Girolamo[**], R. Giacomich[::], A. M. Gorin[••], R. Hess[""], P. Kaustov[**],

K. Kuroda[*], I.V. Manuilov[••], A. Michalowicz[*], C. Newsom[#], K. Okada[:],

K. Okusawa[++], Y. Onel[#], A. Penzo[::], D. Rapin["], G.F. Rappazzo[''], A.V. Riazantsev[••],

V. I. Rykalin[••], G. Salvato['], P. Schiavon[::], D. Sillou[*], M. Slunecka[*o], F. Takeutchi[:],

M. Tareb-Reyes[*] and T. Yoshida[++].

Scintillating fibre technology has made substantial progress, and has demonstrated great potential for fast tracking and triggering in high luminosity experiments in Particle Physics. This talk will present some recent issues of the RD-17 project at CERN for fast and precise readout of scintillating fibre arrays, as well as for upgrade of position-sensitive photomultipliers. Excellent matching of the scintillating fibre and the position-sensitive photomultiplier, in particular in time characteristics, allowed to achieve excellent detector performances, typically a spatial resolution of ~ 125 μm with time resolution better than 1 ns and detection efficiency greater than 95 %.

1. INTRODUCTION

As a photosensitive device the position-sensitive photomultiplier (PSPM) has a number of important features coming from its intrinsic merits, such as high gain, low noise, fast response and high rate capability in addition to simple and reliable operation. In particular, an excellent matching in time characteristics is achieved while combined with scintillating fibres (SciFi) having typically a time response of a few ns. It is worthwhile to mention also the flexible geometry of optical coupling between SciFi and PSPM, that allows a best compromise between different experimental requirements such as the detector size - spatial resolution, the occupancy - number of pixels/tube (= cost effectiveness), and so on.

During 1991 - 1994 the RD-17 Collaboration (FAROS) [1] has achieved several important milestones within the following activities:
• Development and evaluation of upgraded PSPM prototypes based on new grid dynode structure,
• Design and construction of SciFi detector prototypes, and tests of their performance on beam (T7-S at CERN-PS),
• R & D of front-end electronics for real-time processing of track position.

This paper will review some topics in the recent activities [2], and briefly describes the guidelines of upgrading the PSPM, as well as the design concept of SciFi detector for a combined triggering and tracking function.

+	LAPP/IN2P3, Annecy, France	
"	DPNC, University of Geneva, Switzerland	
:	Kyoto-Sangyo University, Japan	
++	Osaka City University, Japan	
•	Charles University, Praha, Czech Republic	
::	Trieste University/INFN, Italy	
o	JINR, Dubna, Russia	

+	CERN, Switzerland
#	University of Iowa, USA
'	Messina University/INFN, Italy
**	Pisa University/INFN, Italy
##	CRN/IN2P3, Strasbourg, France
••	IHEP, Serpukhov, Russia
oo	UCLA, Los Angeles, USA

2. UPGRADE OF PSPM

2.1. Guidelines

The typical structure of the PSPM prototypes is illustrated in Fig. 1. It is characterised by parallel fine grid dynodes with triangular cross section, followed by crossed-wire or pad type anodes.
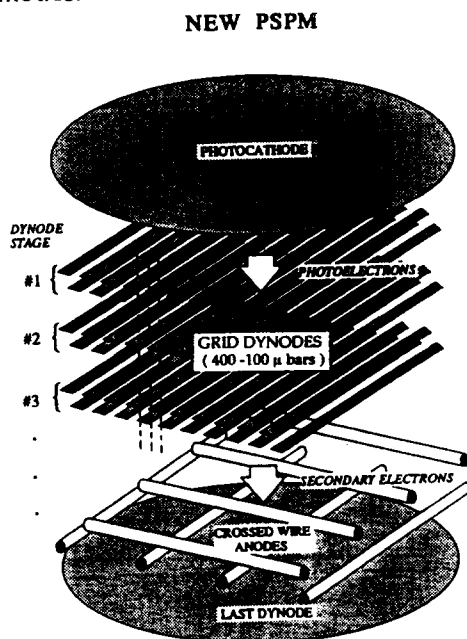
NEW PSPM

Figure 1.Mechanical structure of new PSPM prototypes with crossed-wire anodes.

Each dynode stage consists of two grid layers, the lower one of which is staggered with respect to the upper one by the width of grid bars, so that each stage forms a quasi-opaque structure for primary electrons. This structure ensures a high multiplication factor of secondary electrons per stage, and enhances the possibility of detecting single photo-electrons.

The upgrade of PSPM is carried out along the following guidelines:
- Monte Carlo simulation of secondary electrons,
- Scaling property of electron trajectories.

Fig. 2 shows some typical results of the Monte Carlo simulation taking into account in detail the boundary and initial conditions of each electron trajectory such as, triangular section of the grid bars, energy spectrum, angular distribution of the secondary emission and so on. The distances between grid-layers have been optimised by a compromise between the

gain/stage and the spread of the electron flux at the next dynode levels.

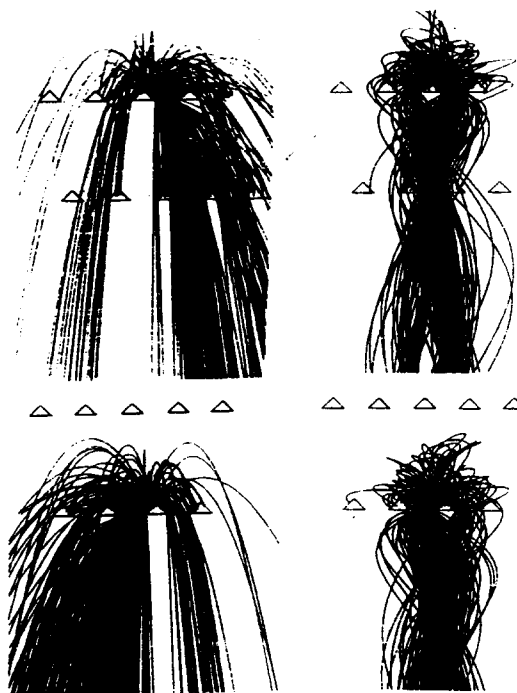a) Without magnetic field   b) With axial magnetic field

Figure 2. Monte Carlo simulation of secondary electrons.

Once the optimal geometry is found, further improvements in spatial and time resolutions can be predicted according to the scaling property of electron trajectories inside electric and magnetic fields [3] - i. e. the Lorentz equation being invariant under a transformation of variables; $r' = r/k_s$, $t' = t/k_s$, $E' = k_s E$ and $B' = k_s B$, a proportional reduction of the dynode structure in 3-dimensions improves the spatial and time resolution by the scaling factor k_s.

2.2. Prototype tubes

Since 1991, several prototype tubes have been conceived and constructed in the framework of RD-17. As listed in Table 1 the dynode structure follows a scaling down of the dynode-bar width from 400 μ (Proto #1) to 100 μ (Protos #5 – #6). The general feature is characterised by a proximity photocathode followed by 12 - 14 stages of grid dynodes and crossed - wire or pad anodes mounted inside a 3" (round or square) glass envelope (see Fig. 3). Some of them have been comparatively evaluated

Table 1. List of PSPM prototypes.

	Proto #1	Proto #2	Proto #3	Proto#4.*	Proto#5*	Proto#6*
Manufacturer	Hamamatsu	Hamamatsu	Hamamatsu	Hamamatsu	MELZ	Hamamatsu
PSPM Type	R3941 Mod-A	R2486 Mod-A	R2486 Mod-B	R3941 Mod-B	FEU-FAROS	R2486 Mod-C
Size & Shape	3in.square	3in. round	3in. round	3in. square	6 cm round	3in round
Q. E. (%)	~ 20	~ 20	~ 20	~ 20	~ 18	~ 20
Fiducial area	58x56 mm^2	40x40 mm^2	40x40 mm^2	58x56 mm^2	36x28 mm^2	58x56 mm^2
Window	Glass	Glass	Glass	Glass	Glass	Opt. Fibre
Dynode Grid-Width	400 μm	200 μm	200 μm	200 μm	100 μm	100 μm
Dynode Material	Bialkali	Bialkali	Bialkali	Bialkali	Bialkali	CuBe
Anode Type	Pads	Crossed wires	Crossed wires	Pads	Pads	Crossed wires
# of stages	14	12	12	12	12	12
# of Anodes	8x24 = 232	16+16 = 32	16+16 = 32	8x29 = 232	8x18 = 144	36(X)+8(Y)
Typical HV(V)	1600	2200	2700	> 2000	>2000	>2000
Gain	~ 10^6	~ 10^6	~ 10^5	~ 10^6	~ 10^6	~ 10^7
Electron spread W0 (FWHM)(1)	~ 8 mm	~ 8 mm (3.6 at 400 G)	~8 mm	~8 mm	~4mm	~4 mm
Anode X-talk(%)	~80	~60	~60	~60	~40	~60
Rise time (ns)	5.5	~3.7	2.6	~3.5	~2	~2
S.E.R.(2)	Difficult	Marginal	Marginal	Possible	Possible	Possible
Bmax(G, axial)	~300	~300	~500	~500	~1000	~1000

(1) Intrinsic Electron Spread (All values at B= 0G, unless specified) (2) Single Electron Response
(*) Expected performances from Scaling property

in the laboratories of the participating groups, and tested on beam at CERN in conjunction with SciFi arrays [4].

2.3. Evaluation of prototypes

The prototypes #2 and #3 provided with 200 μ dynodes have been tested under different conditions in HV, in potential bias (factor k) between 2 layers of each dynode stage, and in axial magnetic field strength (B). Fig.4 presents a typical example of the gain variation as a function of B, observed with Proto #2 at HV=2200 V. With an appropriate bias condition (k = 0.15), the gain increases by a factor ~ 3, as B increases from 0 to 250 G, giving a gain of ~ 5 x 10^6 which is quite comfortable for the detection of weak signals.
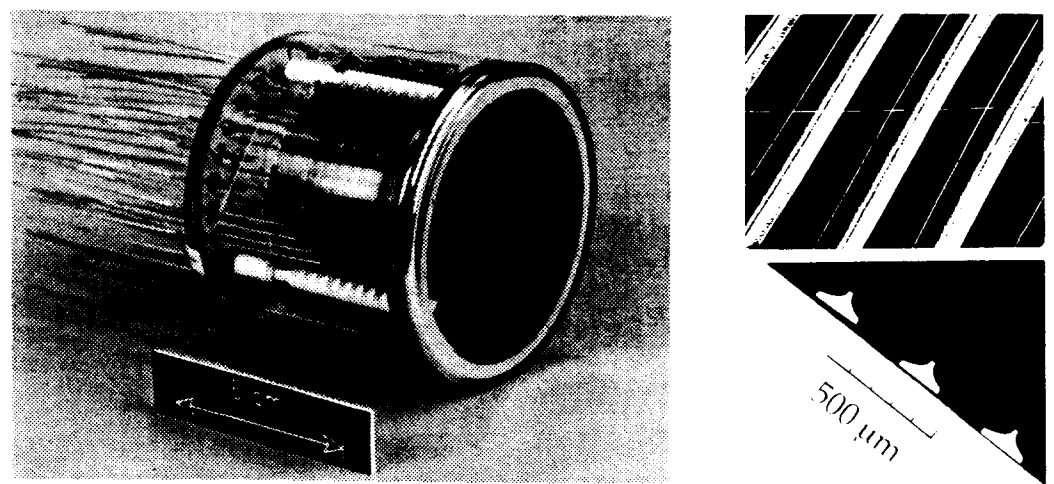

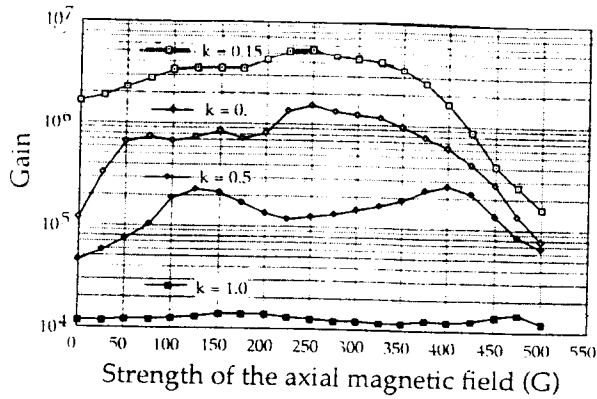Figure 3. Example of new PSPM prototypes with 200 μ grid dynodes.

Figure 4. Gain variation of Proto #2 as a function of axial magnetic field.

The spread of electron flux at the anode level, w_0, has been measured by using a collimated LED. Some results obtained under optimal gain condition are presented in Fig. 5 for different magnetic field strengths.
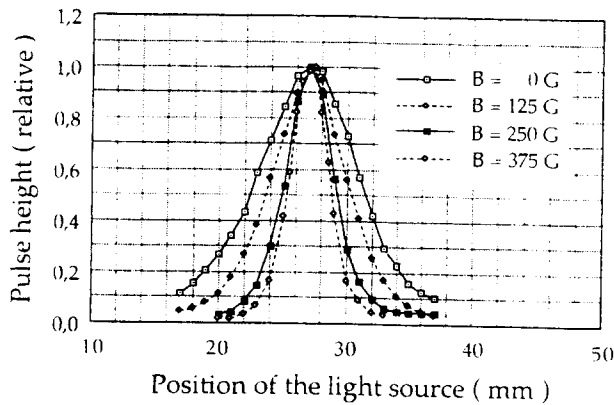

Figure 5. Secondary electron spread at different magnetic field.

The FWHM is ~ 9 mm at B = 0, and shrinks down to ~ 3.5 mm at B = 375 G. Such a shrinkage of the spread is a general behaviour of the PSPM having a parallel grid (or mesh) dynode structure. However, it is worthwhile to mention that a high resolution, say w_0 ~ 3 - 4 mm, is attainable with this prototype without loosing the gain at B = 0. This performance comes essentially from the scale down of the grid size, which enhances secondary electrons escaping from the emitting surface in spite of their spiral motion.

The time characteristics have been studied by using a nitrogen laser source (λ = 337 nm, pulse width = 300 ps) exciting a piece of NE 102A scintillator. The rise time of a commercial tube, for example R2486, is typically ~ 5.5 ns, while we

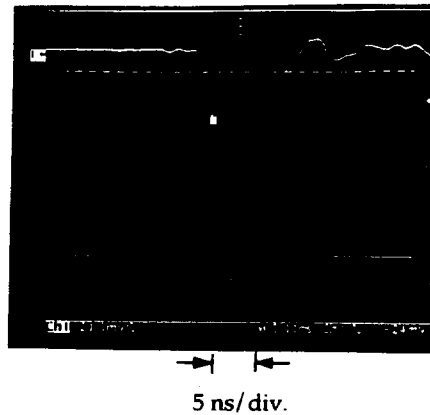measured ~ 3.7 ns for Proto #2, and significantly better for Proto #3 ~ 2.6 ns (Fig. 6).

5 ns/div.

Figure 6. Scope-view of pulses of Proto #3.

Such a performance of the proto-types is close to that of high quality sandard PMT in time characteristics.

The Proto #2 was compared with a commercial tube R2486 in B dependence of the gain and the spread w_0, as shown in Fig.7. The prototype maintains a gain of ~ 10^6 at 400 G, where the gain of R2486 becomes too low to be operational with high resolution, w_0 ~ 3.5 mm.
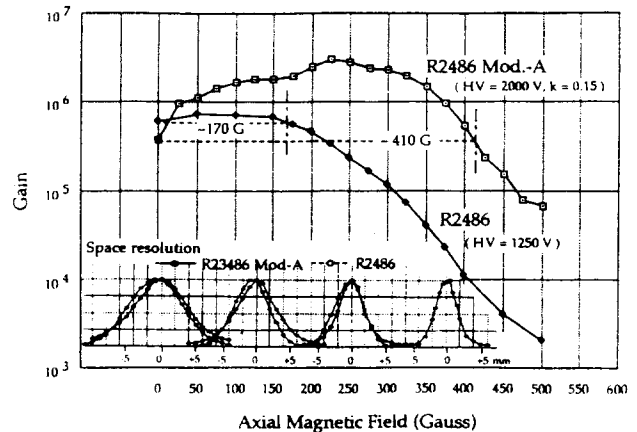

Figure 7. Comparison of Proto #2 to R2486.

An experimental check of the scaling is also achieved by comparing the present data on w_0 with those previously obtained with R1524 [3] (one of the first generation PSPM working inside axial magnetic field); w_0 ~ 10.7 mm in FWHM at HV = 3000 V and B = 150 G. The geometry of the dynode structure of the present prototype is close to that of R1524 scaled down by a factor k_s = 2.5. For HV = 2000 V, the electric field approximately satisfies

the scaling condition, $E' = k_s E$, and at $B' = k_s B \sim 375\,G$ w_0 is ~ 3.6 mm in FWHM. This means that the electron trajectories inside R1524 are proportionally scaled down inside the present prototype by a factor ~ 2.9, which is close to the scaling factor k_s.

3. SCINTILLATING-FIBRE DETECTORS

3.1. Design concept

Readout of individual fibres using multianode PMT, image intensifier followed by CCD, or independent photosensitive devices such as visible light photon-counter (VLPC), is currently considered as "Standard way" of particle tracking by means of SciFi detectors [5].

In spite of recent progress in both SciFi and photosensitive devices this approach seems to suffer still from low light yields of individual fibres and non-negligible cross talk between pixels, those preventing a correct assignment of excited fibres with high efficiency.

In contrast to this trend, RD-17 Collaboration has been investigating another approach [1-2] based on the following viewpoints:
- SciFi bundles can be considered as a "continuous medium" emitting the scintillation light into one direction, and the "average" position of excited fibres is assigned by means of "centre of gravity" or " peak-sensitive" criteria,
- The effective thickness of the medium, i.e. the number of exited fibres along the track, should be defined by taking into account specific conditions of each relevant experiment so that the detection efficiency of each element is close to 100 %. This is the first priority for designing a "topological" trigger device,
- The cross talk should be handled in real time . It is not necessarily an essential nuisance, but often a profitable property for increasing the spatial resolution below the pixel size of the readout device.

A number of prototype hodoscopes have been constructed in this context by using different types of PSPM, such as those having a strong cross talk, "Type A", or a weak cross talk, "Type C", between adjacent elements.

3.2. Type A Hodoscopes using "strong cross talk" PSPM

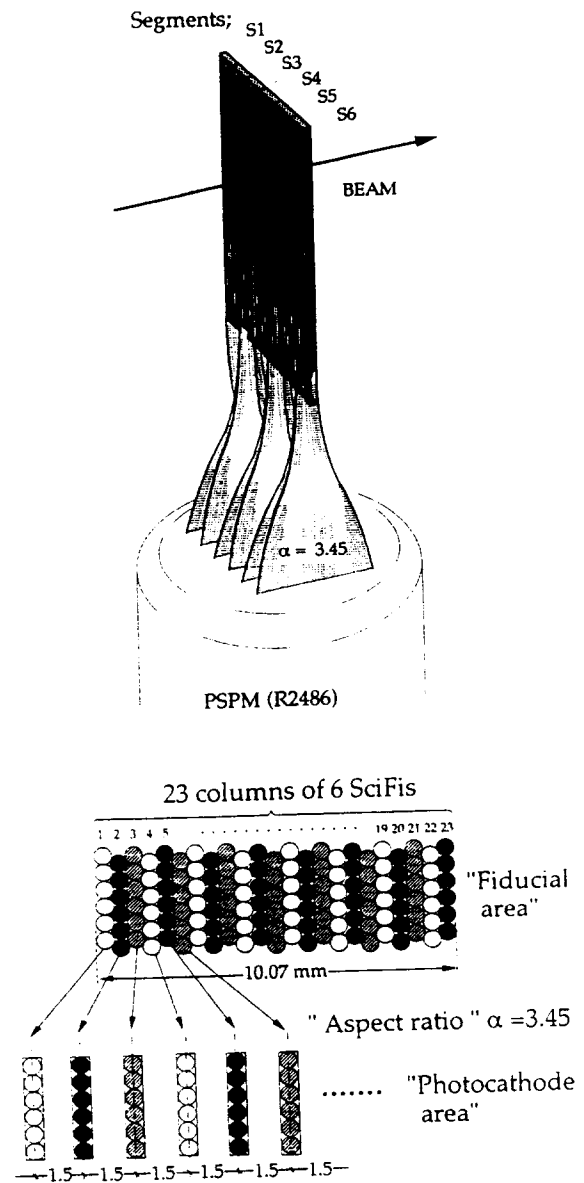Typical example of the mechanical structure is illustrated in Fig. 8

Figure 8. Mechanical structure of Type A hodoscopes.

The SciFi array consists of 6 layers of 0.5 mm φ SciFi (SCS F38 - Kuraray) piled up in "straight" stacking. The sensitive area, 60 mm wide, is split into 6 segments of 10 mm each. The readout edge of each segment is stretched by an "aspect" ratio $\alpha = 3.45$ on the fiducial surface. The stretching is done in practice by locating columns of 6 fibres inside rectangular slots grooved on a disk with

interval of 1.5 mm defining the location of 6 segments on the photomultiplier window.

Most of the present studies have been performed by using a simple delay-line readout circuit [6] illustrated in Fig. 9.
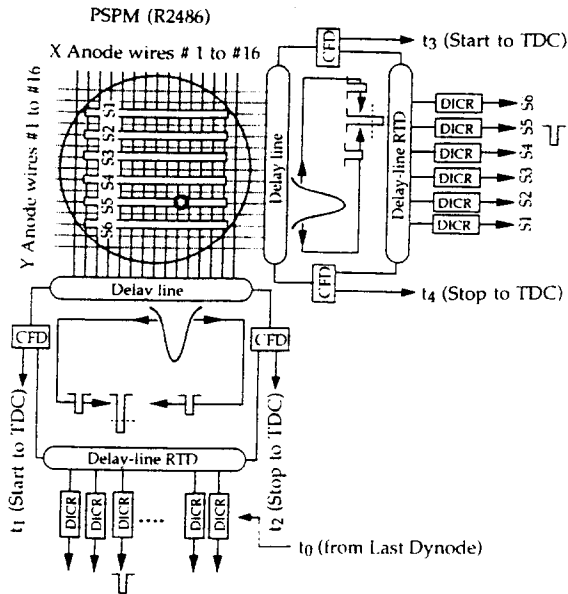

Figure 9. Delay - line electronics.

All the anode wires in one direction (X and Y) are directly connected to a delay line with interval of 3 ns. The position of hit fibres is reconstructed by the time difference between the left and right propagating signals through Time-to-Digital Converters (TDC) or a Real-Time Digitiser (RTD). The latter circuit, specially designed by the RD-17 Collaboration, essentially consists of an array of discriminators, all connected to a second delay line with interval of typically 2.5 ns. The hit position is defined by coincidence of the left and right propagating signals at input of the appropriate discriminator channel. This circuit acts also as a Mean-Timer, suppressing the time fluctuation of the input signals depending on the hit position, thus allowing a sharp strobe to be applied from a common timing channel, for example signals of the last dynode, so that 2-hit events can also be reconstructed.

3.3. Beam-test results of Type A hodoscopes

This type of hodoscope is extensively tested in the T7-S beam at CERN-PS in order to check all the basic properties such as spatial and time resolutions, detection efficiency, double-hit separation and so on.

Fig. 10 presents a typical event distribution in X and Y directions obtained by selecting a certain number of regularly spaced fibre columns seen through a mask on the PSPM photocathode.
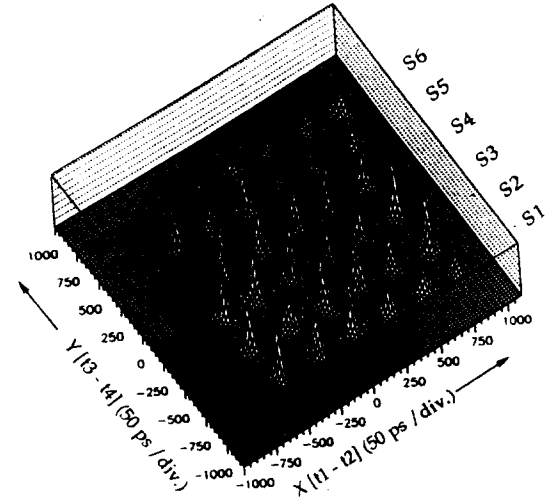

Figure 10. Event distribution obtained with selected SciFi columns.

The spatial resolution, r.m.s. of each peak, is plotted in Fig. 11 as a function of the position of the selected columns. The average value over the full range of 60 mm is $\sigma = 254 \pm 43$ µm.
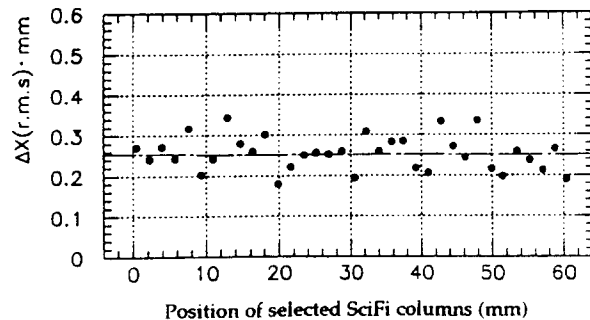

Figure 11. Spatial resolution at different positions.

Improvements in spatial resolution have been confirmed with Proto #2 under magnetic fields, providing preliminary results of $\sigma \sim 130$ µm [7].

The local efficiency was measured by using a finger counter, 0.5 mm wide, defining a partial beam flux entirely passing through the fiducial area of the hodoscope. Fig. 12 presents the number of coincidences between the hodoscope and

the finger counter, normalised to the number of incident particles. This "raw" efficiency was in general close to 100 %, but it is slightly affected by spurious events, the amount of which depends on the incident beam inten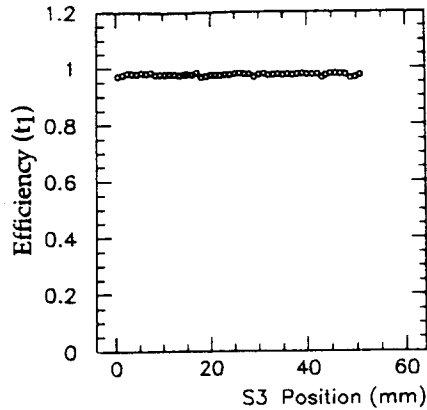sity - under the T7-S beam conditions, the intensity being $< 10^6$ /s, the reconstruction efficiency is estimated to be > 95 %.

Figure 12. Detection efficiency as a function of hit position.

The linearity of the reconstructed position is shown in Fig. 13 for the individual segments , S1 to S6 (open circles) as well as for the full range of the SciFi array. Note that the readout direction of fibres is inverted from segment to segment except for S4 to S5.
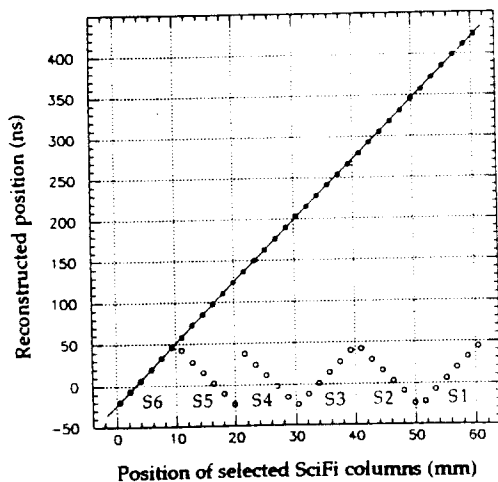

Figure 13. Linearity of reconstructed position ; o : inside segments #1 to #6, • : over full range.

The linearity is quite good with a deviation $\sigma = 74$ µm over the full range.

The two-hit resolution was studied by using two parallel identical SciFi arrays which are separately movable at the fiducial area, but joined at the readout edge on the same position of the PSPM photocathode. The double-hit events were generated in such a way that a shift Δx between the two arrays produces two simultaneous light spots on the photocathode. Single-hit events coming from the non-overlapping parts of the arrays were eliminated with the aid of a small definition counter, 0.3 mm wide, directly mounted onto the fixed array. Fig. 14 presents scope-views of analog pulses coming out of the delay line (upper traces), and the corresponding pulses at the output of CFD (lower traces) for some typical events generated with different separation Δx. The CFD responds corectly when $\Delta x > 3$mm, but below this value it often triggers only once due to a strong overlap of analog pulses. The reconstruction of double-hit events was done in two ways; off-line analysis of TDC data, or real time digitisation of signals from CDF.
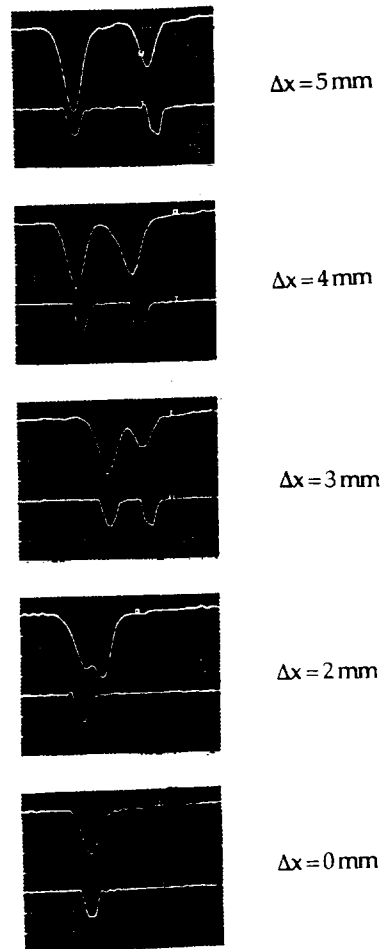

Figure 14. Typical examples of two-hit events with different "track" separation.

Fig. 15 shows results of the real-time reconstruction at different separation Δx. As expected from the scope-views, 2 hits are confused below $\Delta x < 3$mm.
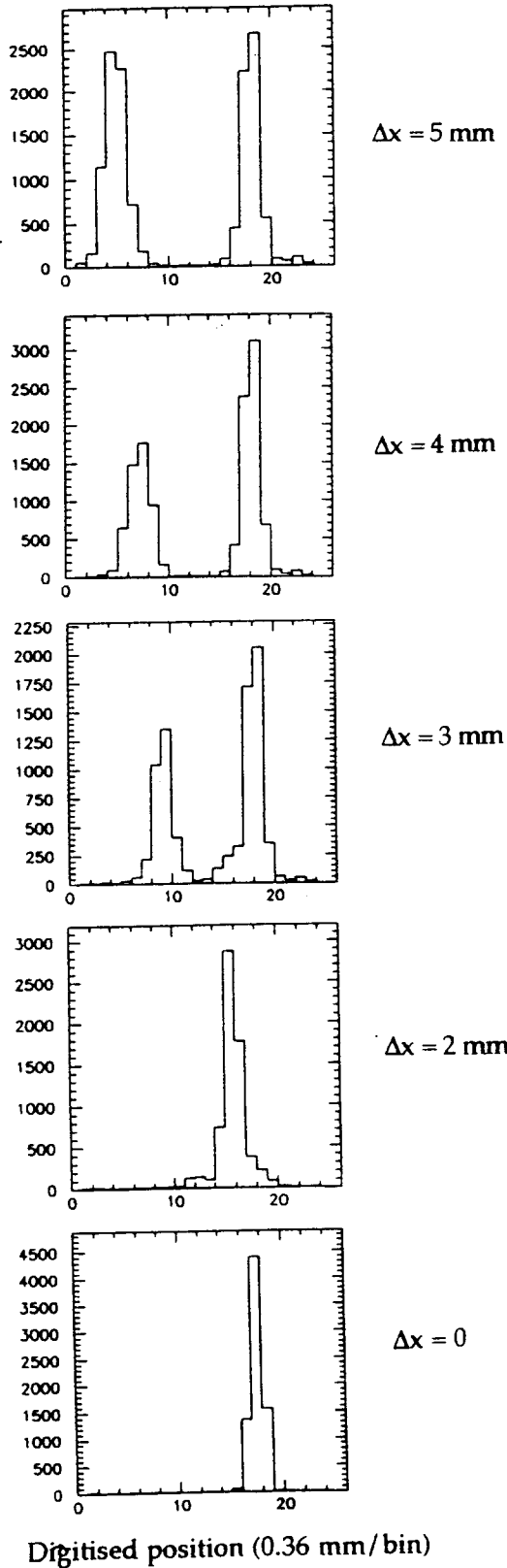
In order to improve the two-hit resolution a "double-side" CFD was recently developped by Okada et al. [8]. This discriminator, triggering at the front and rear edges of analog input pulses, can reproduce the double hits even if they are strongly overlapped. Some preliminary results are shown in Fig. 16 for $\Delta x = 0$ to 2.5 mm. The two-hit resolution is limited here only by the resolution of the individual hits, which was ~ 0.5 mm.

Digitised position (0.36 mm/bin)

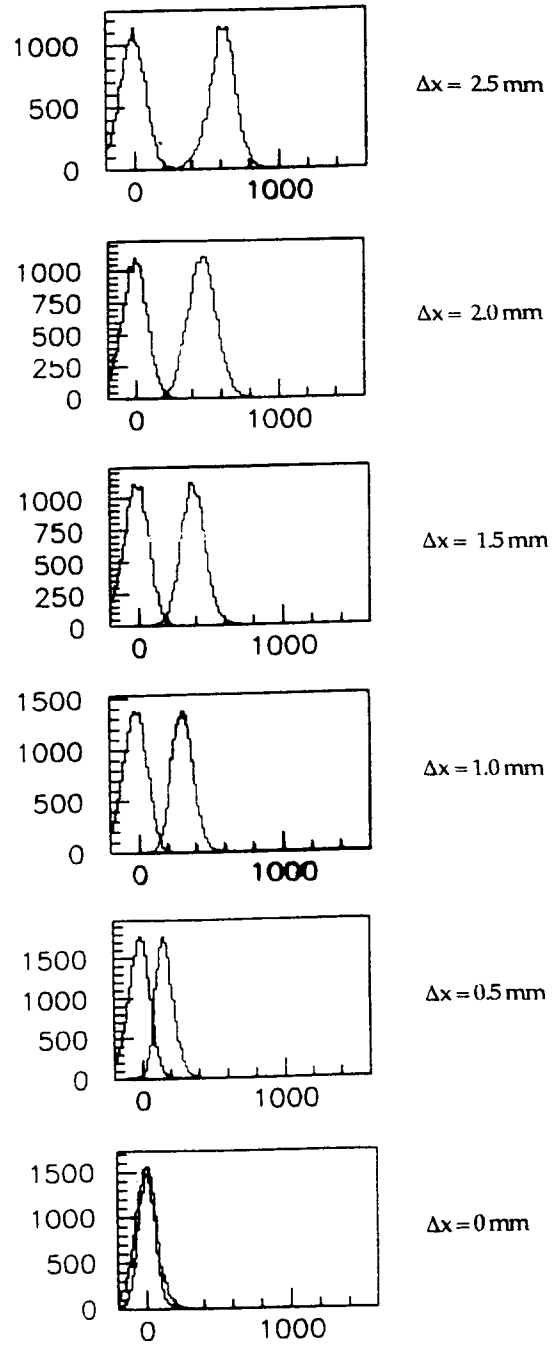Figure 15. Real-time reconstruction of two-hit events using delay-line digitiser.

Figure 16. Reconstruction of two-hit events using "double-side" CFD.

Another important issue concerns the time characteristics of the readout system based on the delay-line. These characteristics were studied by computing the mean time, $(t_1 + t_2)/2$, with respect to a reference time t_0, where t_1 and t_2 are the TDC contents corresponding to the arrival times of the left and right propagating signals coming out of the delay line, and t_0 is generated by either the last dynode of the PSPM or by an external counter. Fig. 17 shows the time-sum distribution with respect to t_0 defined by a beam counter. Assuming that the time resolution of this reference counter is roughly comparable to that of the PSPM the proper resolving time of the hodoscope is estimated to be $\sigma_t \sim 0.8$ ns.
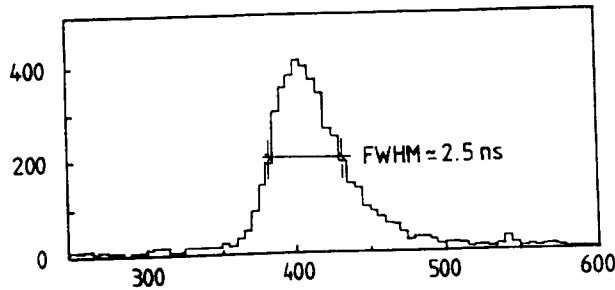

Figure 17. Mean-time, $(t_1+t_2)/2$, distribution with respect to the reference time t_0 defined by an external counter.

3.4. Type C hodoscopes using "weak cross-talk" PSPM

As another application of the design concept presented in Section 3.1., a new prototype of SciFi detector is actually under study in view of constructing a high resolution tracking & trigger detector for a future experiment DIRAC at CERN [9]. The prototype is characterised by a "weak cross-talk (~ 5 %)" PSPM, Philips-XP1724 (provided with optical-fibre window), and a "peak sensitive" front-end electronics [10] which is under preparation at LAPP to complete the prototype in the near future.

As shown in Fig. 18 the SciFi array consists of 32 columns of 5 fibres, 0.5 mm in diameter (CSCF38-Kuraray), aligned perpendicular to the incident particle direction. The effective thickness is therefore ~ 2.5 mm (~ 0.6 % of X_0). The extremity of the columns is fitted onto the

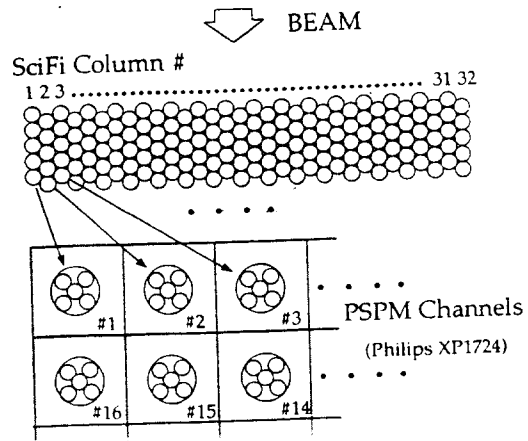centre of corresponding PSPM pixels, each having a size of 2.56 x 2.56 mm^2.

Figure 18. Mapping of SciFi columns onto PSPM channels with weak cross-talk.

Two identical arrays are precisely superposed so that one of them (B) serves as "track-definition" layer to study the performances of the other (A). The layout of the experimental set-up on T7-S beam is illustrated in Fig. 19.
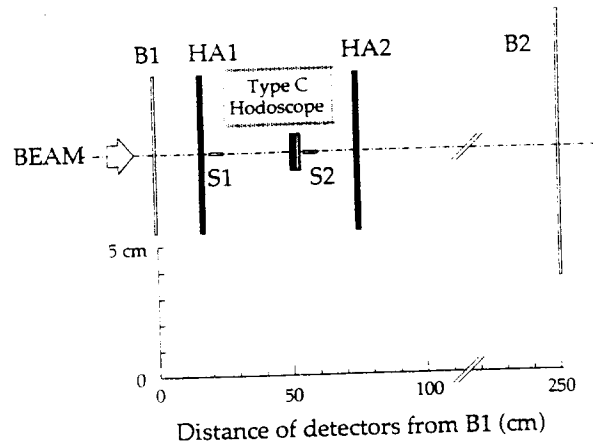

Figure 19. Experimental layout on T7-S.

The prototype is installed between two Type A hodoscopes HA1 and HA2 having a spatial resolution of $\sigma \sim 250$ μm . These hodoscopes, as well as trigger counters S1 and S2 (0.5 mm in lateral width), provide an "external" tracking of incident particles in the final study of the spatial resolution and the detection efficiency. The present test was performed by recording output signals from XP1724 through ADC (44 channels) covering 22 SciFi columns of each A and B layer (see Fig. 20).
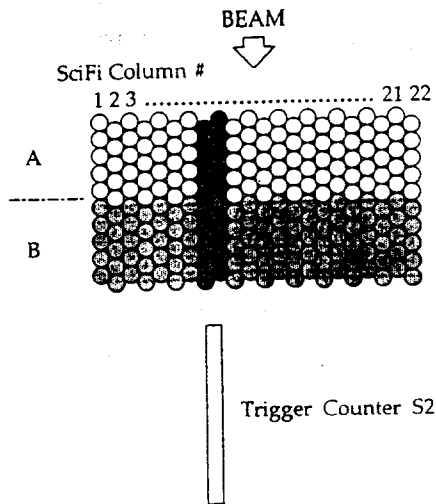
Figure 20. Double SciFi-arrays for "proximity" tracking.

3.5. Preliminary results on Type C hodoscopes

Preliminary results presented here have been obtained by analysing partial data relative to Type C hodoscope only, without external tracking with HA1 and HA2. The incident flux is therefore simply defined by S2 in coincidence with B1.

Preliminary tests of the prototype were carried out in Summer 1994 on T7-S beam at CERN. In this paper we report on a first survey of results issued from a off-line analysis of the partial data.

Fig. 21-a) presents a series of "raw" spectra of successive channels from #A7 to #A10, obtained with S2 placed between #A8 and #A9. The spectra of irradiated channels, #A8 and #A9, are characterised by 3 components: pedestals mainly coming from RF noises, "grazing" tracks (along #A8 and #A9) and "passing-through" tracks. In spite of the incident flux defined by S2, ~ 20 % of events are found in the pedestal region (< 50 - 60 in ADC bins). These events, not exciting the irradiated bins neither in A nor in B, can be considered as background produced by a beam halo hitting both the SciFi bundle and the photocathode window of the S2 counter.

In order to extract the "real" spectrum of passing-through tracks we investigated the following approaches:
• Indirect cut of pedestals by a threshold on the spectrum of B layer,
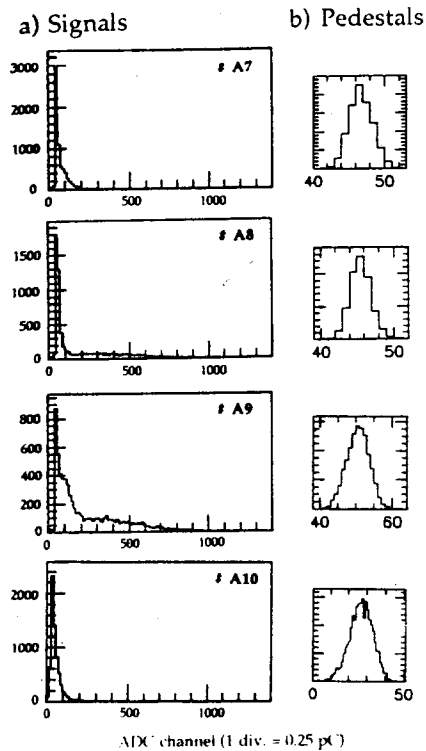• Selection of events by tracking.

Figure 21. "Raw" spectra from adjacent anodes.

The "cleanup" of the spectrum is more efficiently done by selecting events by tracking. In analogy with the peak-sensitive function of the front-end electronics, tracks are defined in this study by the channels giving maximum amplitude in ADC among all the active bins.

Fig. 22-a) and b) present spectra of channels #A8 and #A9 for tracks passing through #B8 and #B9 respectively.

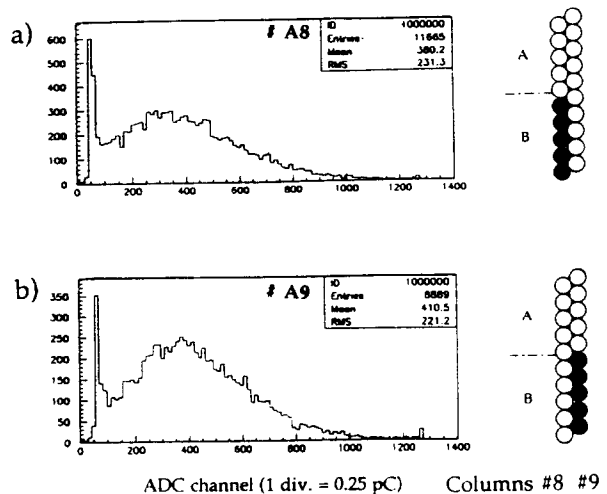ADC channel (1 div. = 0.25 pC)   Columns #8 #9

Figure 22. Spectra after B-layer tracking.

A relatively large tail of the first peak at ADC bins > 50-60 can be interpreted as a contamination mainly coming from grazing tracks due to a finite beam divergence.

Similar results obtained by "double layer" tracking across A and B layers are shown in Fig. 23-a) to d) for different combinations of SciFi columns, as indicated on the right-hand side of each spectrum.

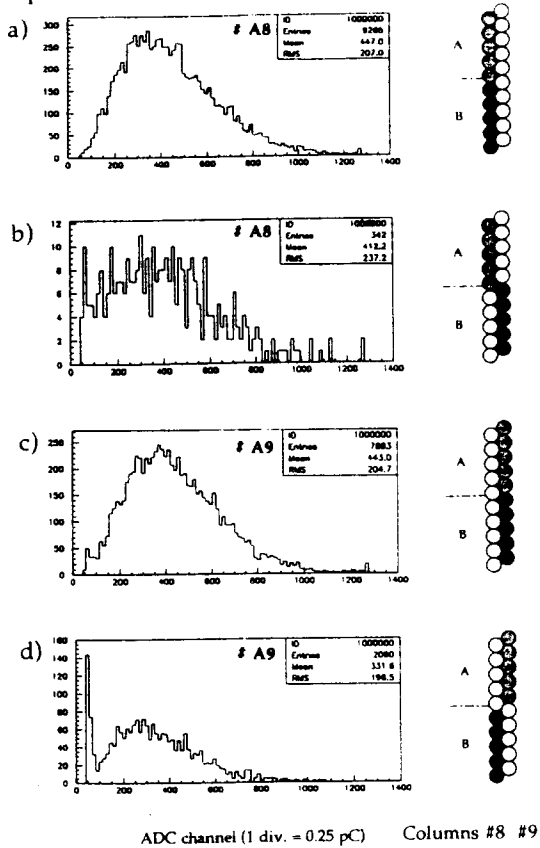ADC channel (1 div. = 0.25 pC)   Columns #8 #9

Figure 23. Spectra after double layer tracking across A and B.

As expected, the pedestals are almost suppressed except in d), where they may produce false assignment of tracks due to the higher pedestal level (see Fig. 21-b) #A9). Much larger number of tracks in this combination (2090 events) compared to that in b) (342 events) means that the average angle of incident particles was slightly inclined as illustrated in Fig. 24-c).

The detection efficiency of A-layer can be roughly estimated from the total numbers of selected events in single- and double-layer tracking. Summing up the numbers of events shown in Fig 22-a) and b), and Fig. 23-a) to d) the efficiency thus defined is;

|Double-layer tracking|/|B-layer tracking| 19590/20554 = 0.953.

More rigorous estimates will be done soon by using data on HA1 and HA2 for external tracking.

Fig. 24 presents track distributions on A-layer after selection of events by;
a) B-layer tracking plus indirect cut of pedestals in #B8 (> 50 in ADC bins), and
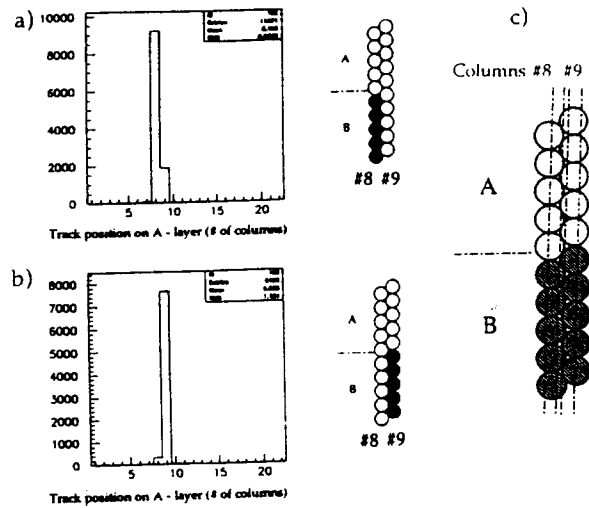b) the same criteria in #B9.

Figure 24. Track distribution in A-layer after tracking in B-layer.

As a matter of fact, the indirect cut of pedestals was rather redundant, because the total number of tracks counted here (19469) amounts to 99.3 % of those defined by the double layer tracking only (19590). The loss of 0.7 % (~120 events) roughly corresponds to the number of pedestal events seen in Fig. 23-d). In Fig. 24-a), ~2000 events in channel #A9 can be considered as inclined tracks passing through #B8 - #A9 in diagonal as illustrated in Fig. 24-c). From Fig. 24-b) one finds that most of events, say > 90 %, selected by B-layer tracking fall inside the corresponding channel #A9. The spatial resolution is therefore estimated to be: = [pitch of SciFi columns (0.43 mm)]$/\sqrt{12}$ = 125 μm.

The time resolution was also measured by using one of PSPM channels. Timing signal (t_1) of this channel thgrough a CFD was registered together with a reference time signal, t_0, from B1 counter. Event distribution as a function of ($t_1 - t_0$) is shown in Fig. 25. The r. m. s. of the distribution is ~1.2 ns including the time resolution of B1, say, ~ 0.5 ns.
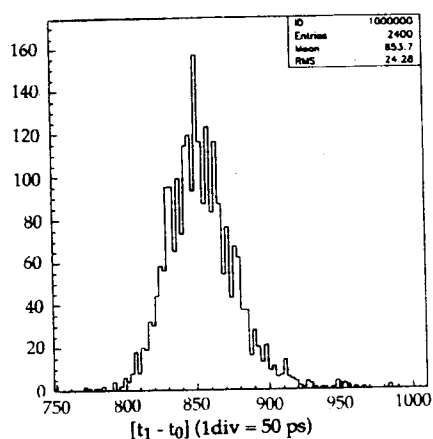
Figure 25. Time distribution of signals from PSPM (XP1724) through CFD with respect to beam counter B1.

The present survey reveals quite encouraging performances of Type C hodoscope, such as:
- Detection efficiency ~ 95 %,
- Spatial resolution ~ 125 μm,
- Time resolution < 1.2 ns.

Within the analogy between the maximum amplitude criterion and a peak-sensitive electronics we consider that the front-end electronics [10] detecting the peak channel among the cluster of adjacent bins has a great advantage compared to the "Standard" electronics consisting of discriminators only. Because, such a circuit should provide, in real time, a correct assignment of excited bins by "absorbing" small nearby pulses originated from the cross talk or electronic noise. In connection to our original approach presented in Section 3.2., it is worthwhile to mention that such a circuit initially conceived for dealing with the strong cross talk will also play a crucial role for "absorbing" the weak cross talk which exists, in general, in any type of multichannel position-detectors.

4. Conclusions

Substantial data on the fast readout of SciFi have been obtained within the framework of RD-17 at CERN.

Upgrade of the PSPM along the scaling property of electron trajectories is confirming its validity with promising results in time characteristics as well as in immunity of gain under axial magnetic fields. This fact allows to expect higher performances of the coming prototypes provided with 100 μ grid dynodes.

The Collaboration investigated also the overall characteristics of SciFi detectors provided with different types of PSPM. The first approach using strong cross talk PSPM can be characterised by its simple readout electronics providing high spatial resolution, significantly better than the electron spread of the PSPM.

The second approach using weak cross talk PSPM reveals also quite promising characteristics in space and time resolutions, although the signal processing in real time is still to be developed.

From these investigations we consider that the scintillating fibres coupled with the position-sensitive photo-multiplier is a potential candidate of future detectors playing simultaneously tracking and topological triggering functions for high luminosity experiments.

References

[1] V. Agoritsas et al., CERN/DRDC 91-8, DRDC/P25

[2] V. Agoritsas et al., RD-17 Status Report, CERN/DRDC 93-47.

[3] K. Kuroda, D. Sillou, F. Takeutchi, Rev. Sci. Instr. 52-3 (1981) 337

[4] A. M. Gorin et al., Nucl. Instr. and Methods A344 (1994) 220

[5] Among several papers see for example B. Abott et al., Nuc. Instr. and Methods A327 (1993)319.

[6] K. Kuroda et al., Nucl. Instr. and Methods A300 (1991) 259

[7] V. Agoritsas et al., To be submitted to Nuc. Instr. and Methods

[8] K. Okada, Private communications

[9] B. Adeva et al., "Lifetime measurement of $\pi^+ \pi^-$ atoms to test low energy QCD predictions ", CERN/SPSLC 95-1, SPSLC/-P284

[10] J. Ditta, Proceeding of "Journées VLSI (Full-Custom)" at Collège de France, 2 Feb. 1994.